



Investigating the potential ability of graphene/polydimethylsiloxane coated magnetic Fe₃O₄ nanoparticles as the adsorbent for the dairy wastewater treatment

Omid Beiktash, Zahra Hejri*, Maryam Omidvar, Hadi Ahmari, Babak Feyzizadeh

Department of Chemical engineering, Quchan branch, Islamic Azad University, Quchan, Iran, emails: za.hejri@iau.ac.ir (Z. Hejri), omid.beiktash@yahoo.com (O. Beiktash), maryam_omidvar@yahoo.com (M. Omidvar), Hadiyahmari@gmail.com (H. Ahmari), b_feizyadeh@yahoo.com (B. Feyzizadeh)

Received 13 July 2022; Accepted 12 June 2023

ABSTRACT

In this paper, the graphene/polydimethylsiloxane coated magnetic Fe₃O₄ adsorbents were fabricated by the chemical co-precipitation method and were used in dairy wastewater treatment. Scanning electron microscopy, Fourier-transform infrared spectrometer, vibrating-sample magnetometry, X-ray diffraction test, and Brunauer–Emmett–Teller were employed to investigate the structure and morphology of the magnetic nanoparticles. The effects of initial chemical oxygen demand (COD) concentration, initial solution pH, temperature, and contact time on wastewater adsorption were systematically studied in batch adsorption experiments. The batch adsorption experiments revealed that increasing adsorbent dosage and contact time, but decreasing temperature and initial COD concentration increased percentage removal. The results indicated that maximum removal was achieved as high as 98.5% using an adsorbent dosage of 25 g/L, pH of 2, and temperature of 45°C. In order to investigate the mechanism and kinetics of the adsorption, experimental data were fitted to some adsorption isotherms and kinetic models. The kinetic data showed that the adsorption processes were associated with the pseudo-second-order mechanism. Also, the equilibrium data were more compatible with the Liu isotherm. The maximum adsorption capacity was measured as 108.7 mg/g at 45°C. The values of thermodynamic parameters (ΔG° , ΔS° , and ΔH°) showed that the adsorption of dairy wastewater molecules onto the adsorbent surfaces was spontaneous, feasible, and endothermic. It is inferred that this magnetic nano-adsorbent can be employed for effective dairy wastewater treatment.

Keywords: Magnetic nano-adsorbent; Adsorption; Isotherm; Kinetic; Poly(dimethylsiloxane)

1. Introduction

The dairy industry is one of the topmost industries among the food industry. One of the problems associated with this industry is high water consumption in the production of milk products such as yogurt, butter, cheese, curd, etc. [1]. Water is also used in processes such as cooling of milk products, cleaning and washing of the processing equipment. This has resulted in increased wastewater generation leading to environmental problems [2]. Production

processes like pasteurization or homogenization produce wastewater with high levels of biological oxygen demand and chemical oxygen demand (COD) along with pathogens and odor [3]. This polluted water must be handled appropriately; otherwise, it pollutes water bodies and causes serious affects on our ecosystem [4]. Therefore, dairy wastewater treatment is essential. Many technologies and methods have been used over the years for treating industries wastewater and the primary focus of the treatment is to remove the organic solvents and remove COD. These methods are

* Corresponding author.

effective in fields of reduction and time, but most of them are expensive. These methods also have disadvantages, such as the generation of chemical sludge by them, which must be treated before disposal into the environment [5–8]. Some of these technologies that have been used for dairy wastewater treatment are activated sludge treatment method, trickling filters, aerated lagoon, facultative lagoons, constructed wetlands, oxidation ditch, anaerobic treatment methods, etc. [9,10]. Although they are effective in treating dairy effluents, but these methods are uneconomical as they consume a lot of power and chemicals.

Therefore, wastewater treatment design, which provides low-cost with additional benefits from the reuse of water, is very desirable [11]. It is widely recognized that the adsorption technique is an effective and economical technique for wastewater treatment which offers simplicity and operation flexibility to produce high quality treated wastewater [12]. Several synthetic and natural adsorbents such as activated carbon, organoclays, films, meshes, sponges, etc., were researched and applied to adsorb contaminations [13–15]. However, the recycling of these adsorbents from water is difficult. Therefore, the possibility of magnetic adsorbent as alternative have been interested to many researchers [16]. With the help of an external magnetic field, the adsorbents after the adsorption of pollutants can be easily recycled from wastewater [17].

Recently, the construction of adsorbents for wastewater treatment based on magnetic nanoparticles has grown significantly. The presence of ferromagnetic components makes it possible to separate the adsorbent by applying a magnetic field. This avoids the use of methods such as filtration and sedimentation, which increase the process cost and may not be effective. The main advantage of this technology is the large amount of wastewater that can be purified quickly using less energy, and not producing contaminants [18]. One of the problems associated with magnetic nanoparticles is their oxidation in air, hydrolysis in aqueous solution and susceptibility to leaching under acidic conditions. Therefore, to improve the quality and efficiency of magnetic nanoparticles, it is necessary to be coated with appropriate compounds [19].

Depending on the type of wastewater, special coatings can be used to coat magnetic nanoparticles. Because, since the effluent of the dairy industry is a type of oily effluent, it is preferable to use super-hydrophobic coatings to coat magnetic nanoparticles.

We now present the brief literature analysis of dairy waste treatment reported earlier to highlight the novelty of this study. Ekka et al. [20] used a hybrid system based on coagulation and adsorption for high-strength dairy wastewater treatment. Results of the study showed that about 68% and 74% of COD was removed by using adsorption and coagulation methods, respectively. Pathak et al. [21] reported the potential ability of rice husk without any modification as a bio sorbent for the adsorption of organic pollutants from dairy wastewater. A removal up to 92.5% was achieved using an adsorbent dosage of 5 g/L, pH of 2, and temperature of 30°C. Falahati et al. [22] studied the dairy wastewater treatment by graphene oxide nanosheets and demonstrated the maximum absorption capacity of the adsorbent was 730 mg/g for total nitrogen, 600 mg/g for total phosphorus, 26,000 mg/g for COD, and 5,500 mg/g for turbidity.

Al-Anazeh [23] explored the potential of using the synthesized nanoparticles of CuONPs as an adsorbent for the treatment of dairy wastewater. According to their results, the highest COD removal percentage, 95%, was achieved with a temperature of 25°C, pH value of 7.5, 1 g of adsorbent, and a contact time of 120 min.

In this paper, we present a new magnetic nanoparticle, coated with a graphene-containing polymer (polydimethylsiloxane) coating. Since dairy wastewater is oily waste, this research, it was tried to use super hydrophobic magnetic adsorbent. Therefore, polydimethylsiloxane doped with graphene was used as a coating of magnetic nanoparticles.

The morphology and composition of the synthesized adsorbents were characterized using scanning electron microscopy (SEM), Fourier-transform infrared (FTIR) spectroscopy, X-ray diffraction (XRD) test, vibrating-sample magnetometry (VSM), and Brunauer–Emmett–Teller (BET). The adsorption properties were evaluated by equilibrium adsorption experiments. The potential ability of these magnetic nanoparticles as the adsorbent for the adsorption of organic pollutants from dairy wastewater was evaluated. The effects of initial COD concentration, pH, adsorbent dosage, solution temperature on adsorption, and the adsorption kinetics, isotherms, and thermodynamic parameters were studied.

2. Experimental set-up

2.1. Materials

Polydimethylsiloxane (PDMS, average Mn ~ 550) was purchased from Sigma-Aldrich (USA). Ferrous chloride and ferric chloride were sourced from Merck Schuchardt OHG (Germany). Acetone, ethanol, and ammonium hydroxide were purchased from Merck (Germany). Graphene nanopowder (11–15 nm) was provided by SkySpring Nanomaterials, Inc., US. Deionized water was obtained by a purification system (Millipore). Wastewater sourced for this research was provided by a local dairy factory. The characteristic of dairy wastewater used in this study is illustrated in Table 1.

2.2. Synthesis of graphene/PDMS coated Fe₃O₄ magnetic nanoparticles

The super-hydrophobic PDMS/graphene coated Fe₃O₄ magnetic nanoparticles were synthesized by this procedure

Table 1
Dairy wastewater characteristics*

Dairy wastewater characteristics	Value
Chemical oxygen demand	375 mg/L
Biological oxygen demand	287 mg/L
Total dissolved solids	653 mg/L
Total suspended solids	876 mg/L
Oil	254 mg/L
Alkalinity	432 mg/L CaCO ₃ equivalent
Conductivity	1,112 mS/cm
pH	7.56

*Taken from the influent primary sedimentation basin of wastewater treatment plant.

(co-precipitation method): At first, 2.5 g of PDMS was stirred in 50 mL of acetone for 30 min to obtain a homogeneous dispersion. Next, 0.1 g of graphene (G) was added to the PDMS solution and sonicated for 30 min to form a homogenous solution. Then, ferrous chloride (2.0 g) and ferric chloride (5.2 g) at the 1:2 weight ratio were added into the PDMS/graphene solution under continuous stirring at 50°C for 1 h to obtain a yellowish colloidal solution. After that, 10 mL of ammonium hydroxide (25%) was added into solution under continuous stirring until the obtained suspension was black. The mixture was stirred at 50°C for 1 h, and then cooled to room temperature. The obtained suspension was then centrifuged at 5,000 rpm for 10 min and the settled particles were washed with DI water and ethanol several times to remove excess chemical reagents, and finally dried in an oven at 90°C for one night. The obtained black precipitate was Fe₃O₄/(graphene/PDMS) nanoparticles and was ready for use.

2.3. Characterization

SEM images were obtained using a JSM-IT500 InTouchScope™ (Japan) scanning electron microscope with an accelerating voltage of 10 kV. For preparation of the SEM images, the material samples were dispersed on a double side conducting tape on an aluminum support, and then coated with a thin film of gold. FTIR was performed by a Nicolet™ iS20 FTIR spectrometer. The specific surface area was measured by using micrometrics, ASAP 2020, surface area and porosity analyzer. The average pore size and total pore volume were also determined. A VSM (Model: 7400 series, Lake Shore, United States) was employed to study the hysteresis loops and the magnetic properties of the magnetite nanoparticles.

2.4. Adsorption study

2.4.1. Batch experiments

The adsorption studies by graphene/PDMS coated magnetic Fe₃O₄ adsorbent was studied by batch method. These studies were done in 250 mL Erlenmeyer flasks containing a fixed amount of adsorbent. The effects of solution pH, contact time, initial COD concentration, and temperature were investigated on adsorption efficiency.

The pH measurement was done by following the electrometric method using a digital pH meter (HMDPHM80, USA). For adsorption tests, at first a certain amount of adsorbent was added to the samples in the Erlenmeyer flask. Then the mixture was taken on a shaker with an agitation speed of 200 rpm at the sufficient time for adsorption. After passing a certain of time, the mixtures were centrifuged and sieved with filter paper and the final COD concentration was determined in the filtrate using Digital Reactor Block (Model DRB 200, HACH, USA) and 4260/50 dual beam spectrophotometer. The effects of various parameters on the percentage removal were observed by varying initial pH of wastewater (2, 3, 4, 5, 6, 7, 8, 9, 10, 11 and 12), adsorbent dosage (5, 10, 15, 20, 25, 30, 35, and 40 g/L), temperature (298, 308, and 313 K), contact time (0–150 min) and initial COD concentration (100, 200, 300, 400, 500, 600, 700, 800 and

900 mg/L). Then, using the following equation, the removal percentage can be obtained [24]:

$$R(\%) = \frac{C_i - C_e}{C_i} \quad (1)$$

where C_i is the initial COD concentration and C_e is the final COD concentration (mg/L). In addition, the COD absorption capacity can be obtained by the following equation [24]:

$$q_{eq} \left(\frac{\text{mg}}{\text{gr}} \right) = \frac{C_0 - C_e}{m} \times V \quad (2)$$

where C_e and C_0 are equilibrium and initial COD concentrations (mg/L), respectively. Also, V is the volume of solution (L), and m is the adsorbent mass (g).

2.4.2. Sorption model analysis

In order to show the adsorption mechanism and steps of process speed control, such as mass transfer and chemical reactions, kinetic models were used to test the experimental data. These models are including non-linear pseudo-first-order, pseudo-second-order, and intraparticle diffusion models. The non-linear pseudo-first-order equation is expressed by Eq. (3) [25,26].

$$\frac{dq_t}{dt} = K_1(q_e - q_t) \quad (3)$$

where q_e and q_t (mg/g) are the absorption capacities at the time of t (min), and K_1 is related to the absorption rate constant (min⁻¹). After integrating and applying the boundary conditions, at $t = 0$, $q_t = 0$ and at $t = t$, $q_t = q_t$, the linear form of the above equation will be as follows [25,26]:

$$\ln(q_e - q_t) = \ln(q_e) - K_1 t \quad (4)$$

The pseudo-second-order equation is expressed as follows [27]:

$$\frac{dq_t}{dt} = K_2(q_e - q_t)^2 \quad (5)$$

where q_e and q_t have the same meaning in Eq. (5). K_2 (g/mg·min) is also the rate constant of the pseudo-second-order model.

The linear form of Eq. (5) is as follows:

$$\frac{t}{q_t} = \frac{1}{k_2 \times q_e^2} + \frac{t}{q_e} \quad (6)$$

The intraparticle diffusion model is expressed the relationship between q_t and $t^{1/2}$ as in Eq. (7) [28]:

$$q_t = K_{id} t^{1/2} + C \quad (7)$$

where K_{id} (mg/g·min^{1/2}) is the intraparticle diffusion rate constant, and C (mg/g) is the constant that indicates the effect of the boundary layer thickness on the amount of intraparticle diffusion.

Non-linear Langmuir, Freundlich, Temkin, Redlich–Peterson and Liu equations were used to model the adsorption equilibrium results and measure the adsorption rate under different conditions. The non-linear Langmuir equation is expressed as follows [29]:

$$\left(\frac{x}{m}\right) = q_e = q_{\max} \left(\frac{b \times C_e}{1 + K_L \times C_e}\right) \quad (8)$$

where (x/m) is the surface coverage fraction (the ratio of the covered surface to the total surface available for adsorption). The parameter K_L is called the Langmuir adsorption equilibrium constant and is a measure of how strongly the adsorbed molecules are adsorbed on a surface. q_{\max} is also the maximum adsorbed COD concentration corresponding to the monolayer coating, and C_e (mol/L) is the equilibrium COD concentration of adsorbate at equilibrium.

The non-linear equation for the Freundlich model is described by Eq. (9) [30]:

$$q_e = \left(\frac{x}{m}\right) = K_f \times C_e^{1/n} \quad (9)$$

where K_f ((mg/g)(mg/L)^{-1/n}) is the Freundlich constant related to adsorption capacity; n is the Freundlich exponent related to the adsorption favorability. If the value of $1/n$ lies in between $(0 < 1/n < 1)$ it shows that isotherm is favorable; if, $1/n = 0$, it indicates isotherm is irreversible, and if, $1/n > 1$, it is unfavorable.

The Temkin isotherm takes into account linear rather than logarithm decrease of the heat of adsorption while ignoring extremely low and very high concentrations. This model assumed that a uniform distribution of binding energy occurred. The Temkin equation is given by Eq. (10) [31]:

$$q_e = \frac{RT}{b_T} \ln A_T C_e \quad (10)$$

where A_T (L/g) is the Temkin constant corresponding to the maximum binding energy, b_T (J/mol) is the Temkin constant related to the heat of adsorption, R (8.314 J/mol·K) is the gas constant, and T (°K) is the absolute temperature.

The Redlich–Peterson model is widely used as a compromise between Langmuir and Freundlich systems. It agrees with the Freundlich and the Langmuir models at the high and low adsorbate concentrations, respectively. The non-linear Redlich–Peterson equation is expressed as in Eq. (11) [32]:

$$q_e = \frac{K_{RP} C_e}{1 + \alpha_{RP} C_e^\beta} \quad (11)$$

where K_{RP} (L/g) and α_{RP} (L/mg) are the Redlich–Peterson isotherm constant, while β is the Redlich–Peterson isotherm exponent.

The Liu isotherm model is the combination of the Langmuir and the Freundlich isotherm models, but some of the assumptions, such as the monolayer assumption of the Langmuir model and the infinite adsorption assumption of the Freundlich model, are negligible. The Liu equation is given below [33]:

$$q_e = \frac{q_m (K_s C_e)^{n_i}}{1 + (K_s C_e)^{n_i}} \quad (12)$$

where K_s is the Liu equilibrium constant (L/mg), and n_i is the Liu model exponent.

2.4.3. Thermodynamic evaluation of dairy wastewater adsorption

Determination of thermodynamic parameters of adsorption is one of the criteria in describing the adsorption process. These parameters (Gibb’s free energy (ΔG° , kJ/mol), standard enthalpy (ΔH° , kJ/mol), and standard entropy (ΔS° , J/mol·K) are expressed using Eqs. (13)–(16) [34].

$$\Delta G^\circ = -RT \ln K_d \quad (13)$$

$$K_d = \frac{C_s}{C_e} \quad (14)$$

$$\Delta G^\circ = \Delta H^\circ - T\Delta S^\circ \quad (15)$$

$$\ln K_d = \frac{\Delta S^\circ}{R} - \frac{\Delta H^\circ}{RT} \quad (16)$$

where R is the gas constant (8.314, J/mol·K), T (K) is the temperature, K_d is the distribution coefficient for the adsorption, C_s is the amount of adsorbed by per adsorbent (mmol/g), and C_e is the adsorbate concentration in solution at equilibrium (mmol/mL). The amounts of ΔH° and ΔS° were obtained by the slope and intercept of the solid line drawn using the plots of $\ln K_d$ vs. $1/T$.

2.4.4. Statistical evaluation of models

The kinetics and isotherm models were evaluated by the adjusted determination factor (R_{adj}^2) and an error function (F_{error}), which is a measure of the differences in the theoretical amount of adsorbate by the adsorbent (q) and the amount measured experimentally. These functions are given below [35]:

$$R_{adj}^2 = \left\{ 1 - \left[\frac{\sum_i^n (q_{i,exp} - \bar{q}_{i,exp})^2 - \sum_i^n (q_{i,exp} - \bar{q}_{i,model})^2}{\sum_i^n (q_{i,exp} - \bar{q}_{i,exp})^2} \right] \right\} \times \left(\frac{n_p - 1}{n_p - p} \right) \quad (17)$$

$$F_{error} = \sqrt{\left(\frac{1}{n_p - p} \right) \cdot \sum_i^n (q_{i,exp} - \bar{q}_{i,model})^2} \quad (18)$$

where $q_{i,model}$ and $q_{i,exp}$ denote the values of q that are predicted by the fitted model and measured experimentally, respectively. Also, $\bar{q}_{i,exp}$ is the average of experimentally measured q , n is the number of experiments performed, and p is the number of parameters of the fitting model.

3. Results and discussion

3.1. Characterization

The SEM image of the sample is illustrated in Fig. 1. It is clear that the PDMS/graphene coated Fe_3O_4 magnetic nanoparticles synthesized in this study had a spherical shape with an average diameter of around 54 nm (Fig. 1a). Also, it is illustrated that the surface of PDMS/graphene coated nanoparticles is rough with wrinkle, which composed of agglomerates of graphene flake. These wrinkles can also be confirmed with an atomic force microscopy image (Fig. 1b and c).

The FTIR spectrums of adsorbent are shown in Fig. 2. In the FTIR spectra of adsorbent before adsorption, the characteristic peaks at $\sim 1,729$; $3,457$ and $2,865$ cm^{-1} are attributed to C=C skeletal vibrations, –OH stretching vibrations

and C–H stretching vibrations of the methylene group of graphene sheets. The peaks at $1,263$; $1,186$ and 753 cm^{-1} , represent the functional groups of Si–CH₃, O–Si–O and Si–(CH₃)₂ of the PDMS molecule. Also, the Fe–O bond stretching vibration at 573 cm^{-1} was observed.

The intensities of the absorption peaks at $1,566$ cm^{-1} (aromatic ring vibration of graphene) are decreased gradually after adsorbing dairy wastewater molecules by adsorbent, suggesting that there was π – π stack effect between PDMS/graphene coated Fe_3O_4 magnetic nanoparticles and dairy wastewater molecules. Also, new characteristic peaks at $2,546$; $1,926$; $1,698$ and $1,634$ cm^{-1} appeared in the FTIR spectrum, indicating that dairy wastewater molecules interact with PDMS/graphene coated Fe_3O_4 magnetic nanoparticles.

Nitrogen adsorption/desorption isotherm studies were carried out by the BET method. Based on nitrogen adsorption/desorption (Fig. 3), Fe_3O_4 magnetic nanoparticles are classified in group II and PDMS/graphene coated Fe_3O_4 magnetic nanoparticles in group IV of this analysis. This isotherm reveals the H₃ hysteresis loop in the range of 0–1 (P/P_0) for both types. The H₃ hysteresis loop is usually associated with slit-like and non-uniform size structures which suggest the mesoporous structure. As shown in Table 2,

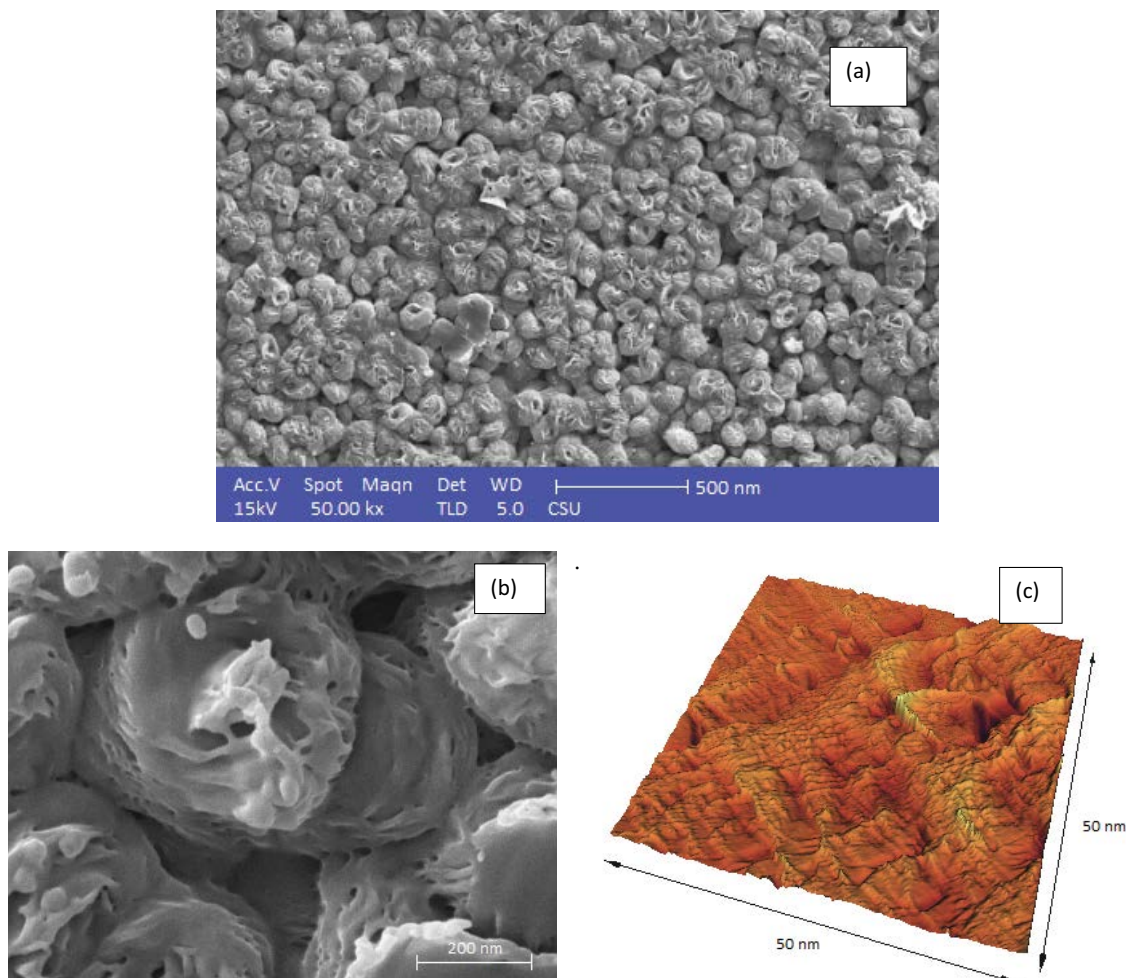


Fig. 1. Scanning electron microscopy and atomic force microscopy image of the PDMS/graphene coated Fe_3O_4 magnetic nanoparticles surface.

there is a clear difference between the active surface of Fe_3O_4 magnetic nanoparticles and PDMS/graphene coated Fe_3O_4 magnetic nanoparticles. In addition, the BET surface area for Fe_3O_4 magnetic nanoparticles and PDMS/graphene coated Fe_3O_4 magnetic nanoparticles is 17.16 and 83.01 m^2/g , respectively. It is indicating that Fe_3O_4 magnetic nanoparticles adhere to each other due to their high magnetic property and bullet shape. So, the active surface will reduce. By coating the nanoparticles with the PDMS/graphene, the particle interactions between the iron oxide nanoparticles are reduced and the agglomeration of these nanoparticles is reduced.

The PDMS/graphene coated Fe_3O_4 magnetic nanoparticles exhibit a broad pore size distribution from 2 to 8.0 nm. The mesoporous structure of Fe_3O_4 nanoparticles and the large surface area of graphene in the adsorbent structure cause a significant increase in adsorption efficiency.

The magnetic property of prepared Fe_3O_4 magnetic nanoparticles and PDMS/graphene coated Fe_3O_4 magnetic nanoparticles was measured by a VSM. Fig. 4 shows the hysteresis loops of these nanoparticles at room temperature. As can be seen, for both prepared nanoparticles, the magnetization reduces from a plateau state to zero on removal of the magnetic field, which is evidence that the prepared nanoparticles are superparamagnetic. Also, the $M_s \approx 73.5$ emu/g, $M_r \approx 0.79$ emu/g and $C_e \sim 2.3$ Oe were obtained for nude Fe_3O_4 magnetic nanoparticles while for PDMS/graphene coated Fe_3O_4 magnetic nanoparticles these parameters (M_s , M_r and C_e) were obtained 34.4 emu/g, 0.49 emu/g and 0.31, respectively. It is concluded that the magnetic property of nanoparticles after coating was reduced by comparing the values of nude nanoparticles. Nevertheless,

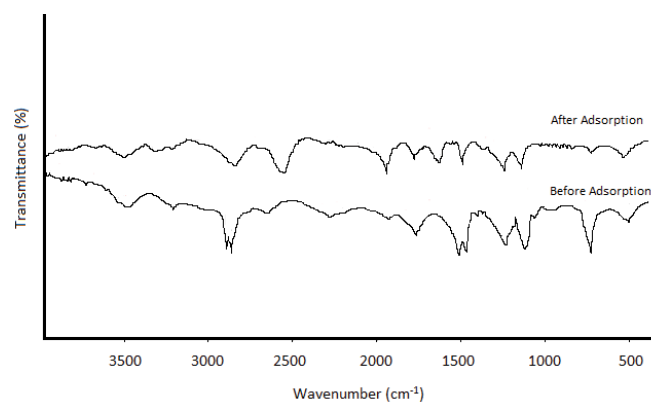


Fig. 2. Fourier-transform infrared spectra of PDMS/graphene coated Fe_3O_4 magnetic nanoparticles before and after dairy wastewater adsorption.

Table 2:

Textural properties of Fe_3O_4 magnetic nanoparticles and PDMS/graphene coated Fe_3O_4 magnetic nanoparticles

Adsorbent	Total surface area (m^2/g)	Total pore volume (cm^3/g)	Average pore diameter (nm)
Fe_3O_4 magnetic nanoparticles	17.16	0.151	24.6
PDMS/graphene coated Fe_3O_4 magnetic nanoparticles	83	0.121	5.4

prepared nanoparticles have proper behavior and can be used in adsorption applications.

The XRD spectra of the Fe_3O_4 MNPs (magnetic nanoparticles) and PDMS/graphene coated Fe_3O_4 magnetic nanoparticles is shown in Fig. 5. The Fe_3O_4 MNPs exhibit the intensity peak at $2\theta = 30.3^\circ, 36.6^\circ, 42.0^\circ, 54.1^\circ, 55.9^\circ,$ and 61.5° . All these diffraction peaks are indexed to the magnetic cubic structure of Fe_3O_4 (JCPDS 19-0629) corresponding to the (220), (311), (400), (422), (511), (440) lattice planes, respectively. For the XRD pattern of PDMS/graphene coated Fe_3O_4 magnetic nanoparticles, it can also be observed that there are the distinct peaks at $2\theta = 11.41^\circ$ and 25.1° which attributed to the PDMS crystal plane and graphene, respectively, indicating that the PDMS/graphene coating is well covered on the Fe_3O_4 MNPs. Also, the XRD pattern of PDMS/graphene coated Fe_3O_4 magnetic nanoparticles at 2θ of $30.3^\circ, 36.6^\circ, 42.0^\circ, 54.1^\circ, 55.9^\circ,$ and 61.5° are smooth. This phenomenon indicates that the characteristic diffraction peaks of Fe_3O_4 MNPs are covered by graphene and PDMS.

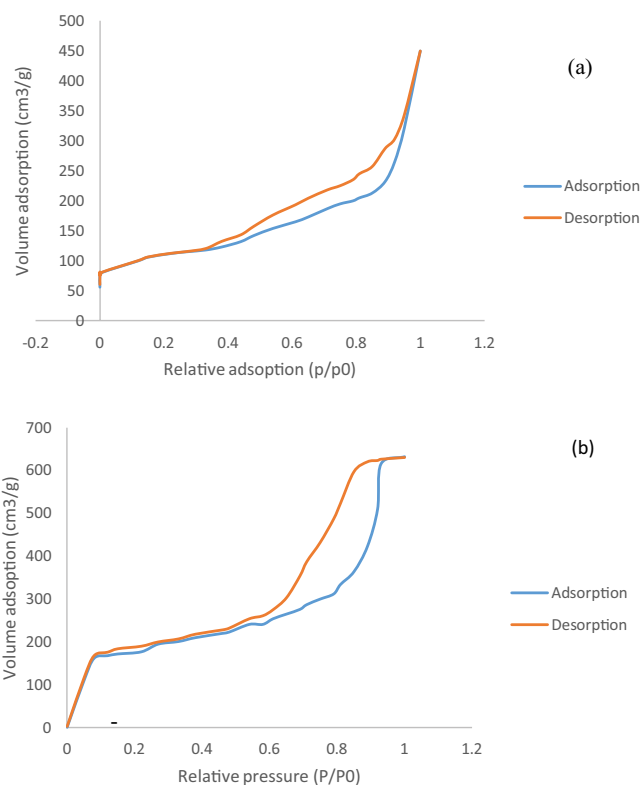


Fig. 3. Nitrogen adsorption–desorption isotherms for (a) Fe_3O_4 magnetic nanoparticles and (b) PDMS/graphene coated Fe_3O_4 magnetic nanoparticles.

3.2. Batch experiments

3.2.1. Effect of adsorbent dosage

The effect of the adsorbent dosage on the adsorption process is shown in Fig. 6. According to the figure, the percentage removal increases with increasing the adsorbent dosage, which is due to the increase in specific surface area and more adsorption sites. With increasing the adsorbent dosage up to 25 g/L, the percentage removal increases rapidly, after which there was no further increase up to 40 g/L. The reason for staying constant is to reach the equilibrium adsorption capacity at higher adsorbent dosage. The adsorbent concentration of 25 g/L is considered the optimal dosage in subsequent experiments.

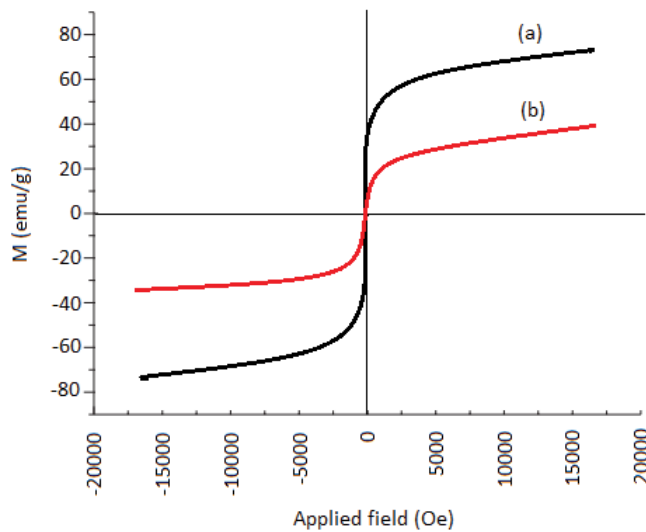


Fig. 4. Vibrating-sample magnetometry curves for the prepared (a) Fe₃O₄ magnetic nanoparticles and (b) PDMS/graphene coated Fe₃O₄ magnetic nanoparticles.

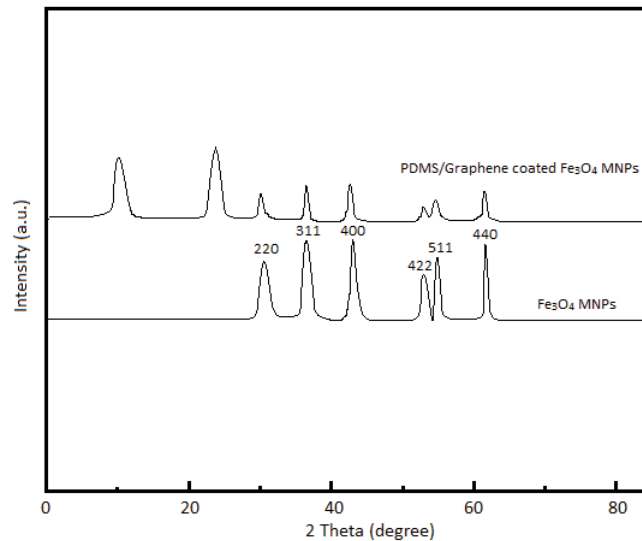


Fig. 5. X-ray diffraction patterns of Fe₃O₄ nanoparticles and PDMS/graphene coated Fe₃O₄ magnetic nanoparticles.

3.2.2. Effect of initial COD concentration

The wastewater initial COD concentration effect on the percentage COD removal at pH = 7.56, contact time of 60 min, and the optimal adsorbent dosage of 25 g/L is shown in Fig. 7. It was observed that by increasing the initial COD concentration from 100 to 200 mg/L, the removal efficiency increases and then by further increasing, the percentage removal decreases. It is due to the increase of the driving force to overcome the total resistance resulting from the transfer of mass between the liquid and solid phases (adsorbent). As the COD concentration increases, despite the greater driving force, the adsorption efficiency decreases due to the saturation of the adsorption sites by the adsorbent.

3.2.3. Effect of initial pH

Fig. 8a shows the potential of the graphene/PDMS coated Fe₃O₄ MNPs under different pH conditions. It was concluded that the zeta potential is positive when the pH is less than 4.7, and negative when pH is more than 4.7. Also, Fig. 8b shows the effect of initial pH on percentage removal by graphene/PDMS coated Fe₃O₄ MNPs. It is evident that the

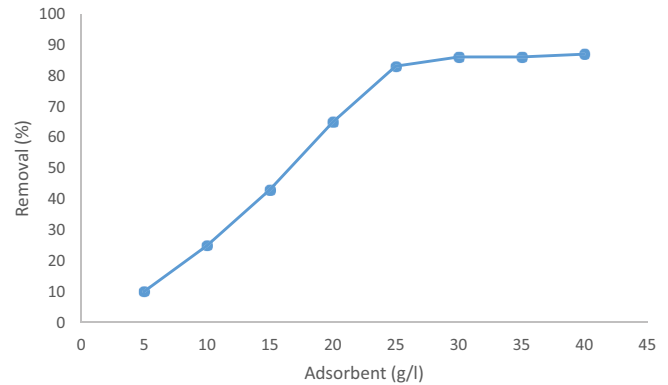


Fig. 6. Effect of adsorbent dosage on percentage removal by the graphene/PDMS coated Fe₃O₄ MNPs (*T* = 25°C, agitation speed: 250 rpm, pH: 7.56).

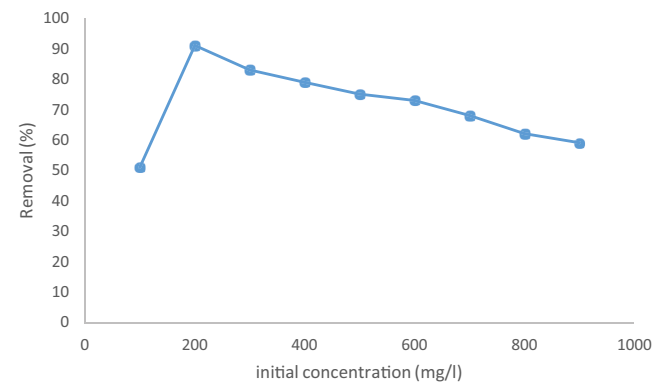


Fig. 7. Effect of initial chemical oxygen demand concentration on percentage removal by the graphene/PDMS coated Fe₃O₄ MNPs (*T* = 25°C, agitation speed: 250 rpm, pH: 7.56).

percentage removal is significantly decreased from 69.5 to 6.1 mg/g by pH increasing up to 10. The adsorbent surface at low pH_{zpc} values would be protonated, which enhances the interactions between the organic substances and binding sites through attractive forces. On the other hand, the milk protein has a negative charge in milk suspension, resulting in the electrostatic repulsion due to the reduction of electrostatic force of attraction between the oppositely charged adsorbate molecules and the adsorbent binding sites in alkali medium.

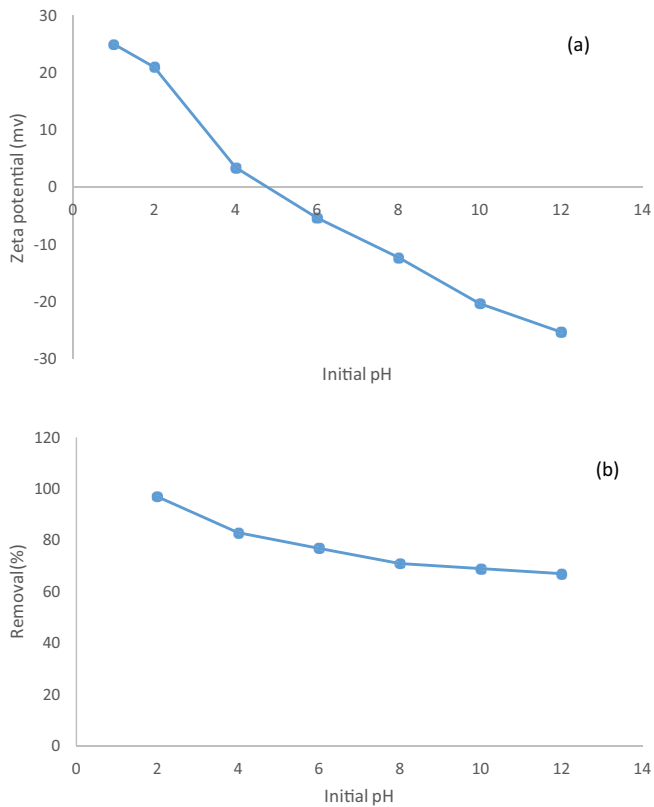


Fig. 8. Effect of solution pH on (a) zeta potential of the adsorbent and (b) percentage removal by the graphene/PDMS coated Fe_3O_4 MNPs ($T = 25^\circ C$, agitation speed: 250 rpm).

3.2.4. Effect of the contact time

The effect of contact time on the percentage removal by the graphene/PDMS coated Fe_3O_4 MNPs is shown in Fig. 9. In the adsorption process, the equilibrium time is considered as the time when the adsorption efficiency is constant and does not change significantly over time. According to Fig. 9, it turns out that the adsorption capacity of the graphene/PDMS coated Fe_3O_4 MNPs towards dairy wastewater increased drastically at the first 50 min, then rose constantly at a relatively slow speed, and finally remained constant. It can be attributed to the frequency of active sites at the beginning of the process. Over time, the adsorption sites on the adsorbent are occupied, and the process slows down and eventually tends to be almost constant, so that more time has little effect on the adsorption rise. The amount of absorption reaches its maximum in the first 50 min and does not change much after that.

3.2.5. Effect of temperature

Fig. 10 shows the effect of temperature on COD removal and the adsorption capacity of dairy wastewater by the synthetic adsorbents. As can be seen, for all of adsorbents, with the increase in temperature, the absorption capacity and

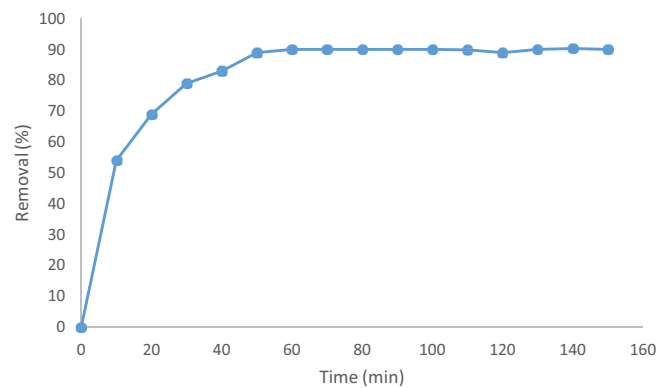


Fig. 9. Effect of contact time on the adsorption of dairy wastewater by the graphene/PDMS coated Fe_3O_4 MNPs ($T = 25^\circ C$, agitation speed: 250 rpm, $pH = 7.56$).

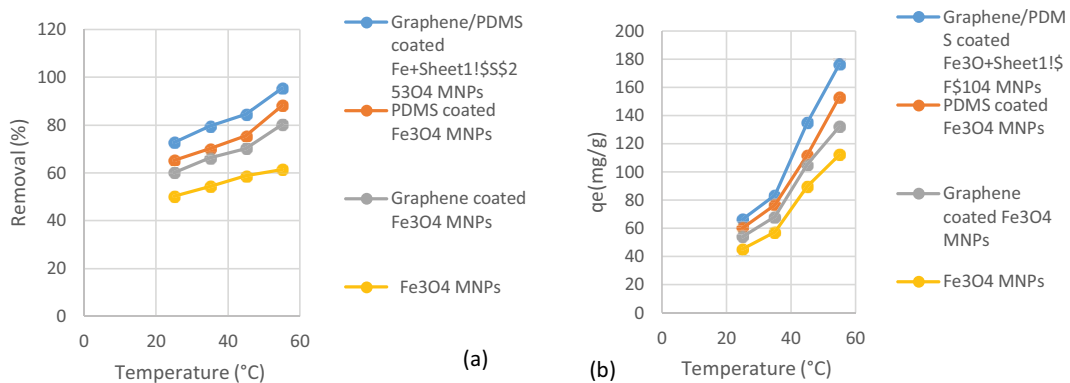


Fig. 10: Evaluation of temperature on (a) percentage removal and (b) adsorption capacity of dairy wastewater by the graphene/PDMS coated Fe_3O_4 MNPs, PDMS coated Fe_3O_4 MNPs, graphene coated Fe_3O_4 MNPs and Fe_3O_4 MNPs (agitation speed: 250 rpm, $pH = 7.56$).

then COD removal increases. For example, for the graphene/PDMS coated Fe₃O₄ MNPs, with increasing temperature up to 55°C, the percentage of COD removal increases from 72.8% to 95.56%. Also, the adsorption capacity reached the maximum value of 176.7 mg/g at 55°C, which indicates that the adsorption process is endothermic. It might be explained by the fact that, at higher temperatures, the diffusion rate of wastewater molecules increases, and more molecules

can interact with the active adsorption sites of adsorbents, owing to the decrease of the solution viscosity along with the increasing temperature.

3.3. Adsorption isotherms

The relationship between adsorption capacity by adsorbent and the concentration of solute in solution at

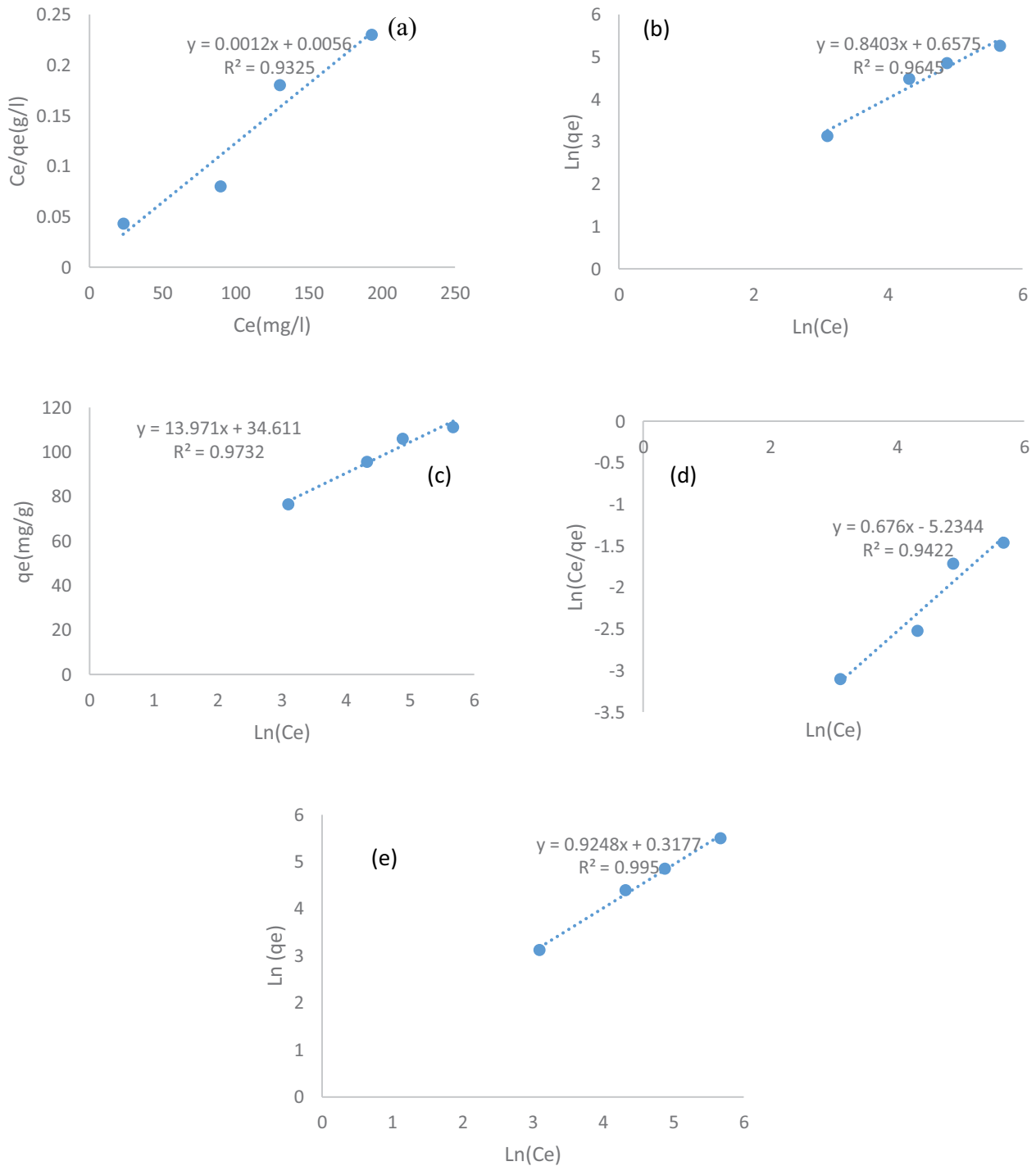


Fig. 11. Linear isotherm models of dairy wastewater adsorption on graphene/PDMS coated Fe₃O₄ MNPs (pH 7.56, adsorbent dose: 25 g/L, T = 25°C ± 1°C), (a) Langmuir, (b) Freundlich, (c) Temkin, (d) Redlich–Peterson and (e) Liu.

equilibrium is quantitative analyzed using absorption isotherms. Investigation of adsorption isotherms is necessary for the design of absorption systems. Herein, the isotherm data were fitted to Langmuir, Freundlich, Temkin, Redlich–Peterson, and Liu models. These models are expressed in the linear form as Eqs. (19)–(23), respectively [36].

$$\frac{C_e}{q_e} = \frac{1}{K_L q_{\max}} + \frac{C_e}{q_{\max}} \quad (19)$$

$$\ln q_e = \frac{1}{n} \ln C_e + \ln K_F \quad (20)$$

$$q_e = \left(\frac{x}{m} \right) = \frac{RT}{b_T} \ln A_T + \frac{RT}{b_T} \ln C_e \quad (21)$$

$$\ln \left(\frac{C_e}{q_e} \right) = \ln \left(\frac{\alpha_{RP}}{K_{RP^2}} \right) + \beta \ln C_e \quad (22)$$

$$\ln q_e = \ln q_m^2 K_S^{n_i} + n \ln C_e \quad (23)$$

The plot of the linear forms of the above-mentioned isotherm models are presented in Fig. 11, and the calculated isotherm parameters along with correlation coefficient (R^2) are listed in Table 3. By comparing, the isotherms data from the table, the higher correlation coefficient (R^2), and lower SD values of Liu isotherm than other isotherms, implying the adsorption of dairy wastewater onto graphene/PDMS coated Fe_3O_4 MNPs can well follow the Liu isotherm model. This model predicts that the active sites of the adsorbent cannot have the same energy. Therefore, the adsorbent may have active sites preferred by the adsorbate molecules for occupation; considering various functional groups on the graphene/PDMS coated Fe_3O_4 MNPs our results shows that the active sites of the graphene/PDMS coated Fe_3O_4 MNPs will not have the same energy.

As can be seen from Table 3, the maximum adsorption capacities based on the Langmuir model enhanced with increasing solution temperature, which is an indicator of the endothermic nature of the adsorption of dairy wastewater by the graphene/PDMS coated Fe_3O_4 MNPs surfaces. The β value obtained from Redlich–Peterson model is greater than one, which confirms the invalidity of this model. Also, the value of the R^2_{adj} obtained from the Temkin model was low for all studied temperatures. This means that the Temkin model is unsuitable for describing the adsorption equilibrium process.

3.4. Adsorption kinetic analysis

In order to study the mechanism of dairy wastewater adsorption, the experimental kinetic data were fitted using the kinetic models (pseudo-first-order, pseudo-second-order, and intraparticle diffusion models). The results of kinetic data are presented in Fig. 12 and Table 4.

As can be seen from the comparison of correlation coefficients, the pseudo-second-order model is more appropriate in predicting the rate of the adsorption process.

Also, the q_e value predicted for this model was close to the experimental one. In the pseudo-second-order model, the rate-limiting step corresponds to chemisorption, which is based on valence forces generated by sharing or exchanging electrons between the adsorbent and adsorbate.

The Weber’s intraparticle diffusion model was used to study the kinetic mechanism of dairy wastewater onto the graphene/PDMS coated Fe_3O_4 MNPs surface. The plot of q_t vs. $t^{1/2}$ shows two linear regions, indicating two steps exist during the adsorption process. The first and sharper region is related to the external diffusion of dairy wastewater molecules, while the second region attributes to the diffusion of dairy wastewater molecules into the less accessible pores of adsorbent, where intraparticle diffusion was the rate-limiting step.

The intraparticle diffusion rate constant (K_{id}) value for step I and II was determined from the slope of each curve. As can be seen, the slope of the first linear region was much higher than rate constant of the second step, indicating that intraparticle diffusion controls the adsorption rate mainly. However, external mass transfer resistance cannot be neglected, although this resistance is only significant at the initial time.

3.5. Thermodynamic analysis

The plot of $\ln(K_d)$ vs. $1/T$ is illustrated in Fig. 13, and the results of thermodynamic data are presented in

Table 3
Isotherm parameters for adsorption of dairy wastewater by graphene/PDMS coated Fe_3O_4 MNPs at different temperatures

Adsorption isotherm model	Parameters	Temperature (°C)		
		25	35	45
Langmuir	q_{\max} (mg/g)	81.72	93.61	107.93
	K_L (L/mg)	0.220	0.312	0.394
	R^2	0.932	0.901	0.921
	F_{error}	0.61	0.65	0.63
Freundlich	K_f (L/g)	1.92	2.32	3.41
	n	1.19	1.15	1.13
	R^2	0.964	0.953	0.935
	F_{error}	0.71	0.74	0.78
Temkin	A_T (L/g)	11.82	13.32	15.34
	b_T (J/mol)	177.21	181.22	185.45
	R^2	0.973	0.932	0.914
	F_{error}	0.54	0.51	0.58
Redlich–Peterson	K_{RP} (L/g)	2.41	4.43	7.76
	α_{RP} (L/mg)	0.98	0.81	0.74
	β	1.67	1.82	2.13
	R^2	0.942	0.922	0.902
Liu	F_{error}	0.43	0.65	0.53
	q_{\max} (mg/g)	85.91	98.73	108.71
	K_S (L/mg)	0.006	0.009	0.012
	n_i	0.92	1.22	1.45
	R^2	0.995	0.990	0.971
	F_{error}	0.32	0.28	0.30

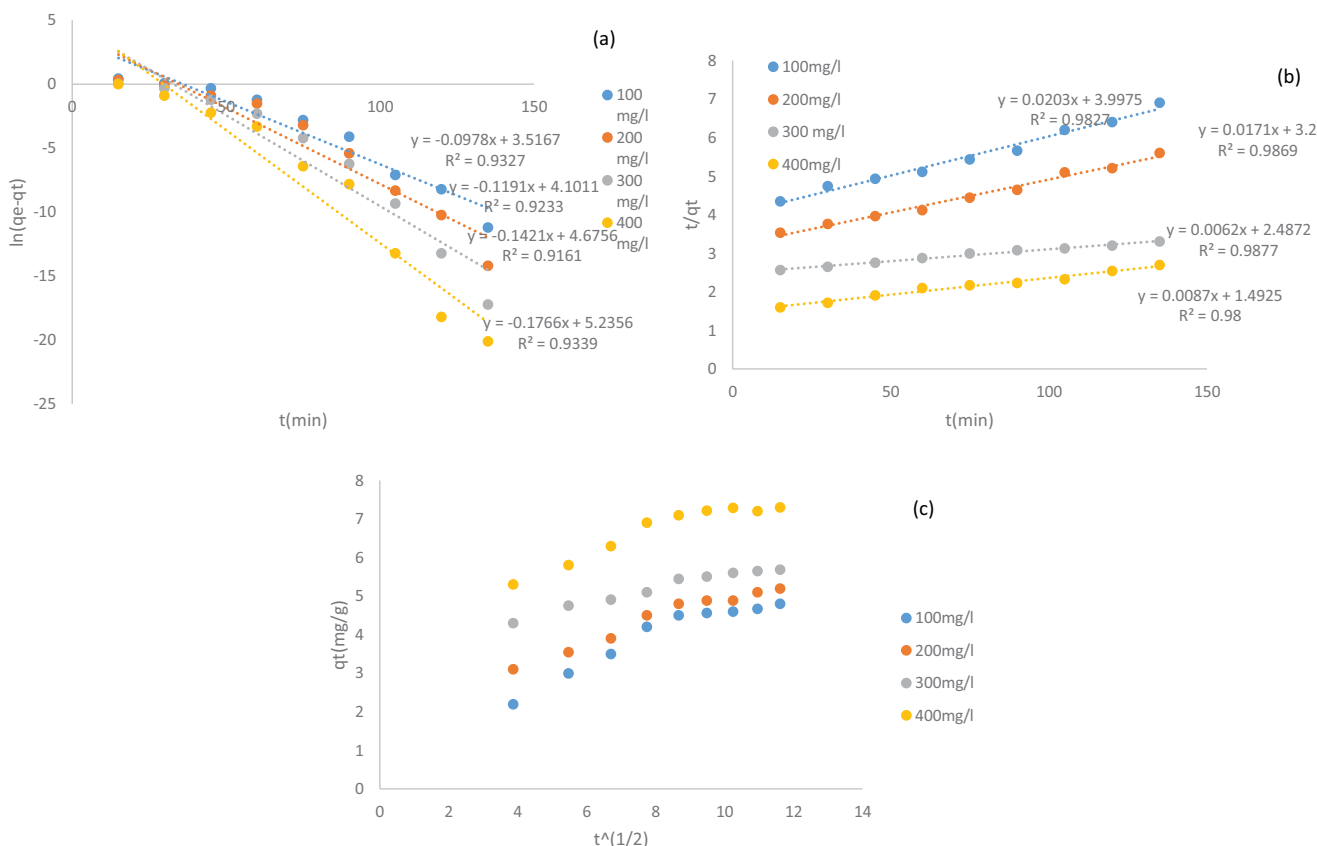


Fig. 12. Linear kinetic models of dairy wastewater adsorption on graphene/PDMS coated Fe_3O_4 MNPs (pH 7.56, adsorbent dose: 25 g/L, $T = 25^\circ\text{C} \pm 1^\circ\text{C}$), a) pseudo-first-order, b) pseudo-second-order and c) intraparticle diffusion models.

Table 4

Kinetic parameters for adsorption of dairy wastewater by graphene/PDMS coated Fe_3O_4 MNPs at different chemical oxygen demand concentrations

Adsorption kinetic model	Parameters	Initial chemical oxygen demand concentration (mg/L)			
		100	200	300	400
Pseudo-first-order	q_e (mg/g)	33.11	60.12	99.21	181.10
	K_1 (min^{-1})	0.09	0.11	0.14	0.17
	R^2	0.931	0.920	0.911	0.934
	F_{error}	0.91	0.87	0.77	0.75
Pseudo-second-order	q_e (mg/g)	50.23	58.81	111.11	166.12
	K_2 (g/mg-min)	0.0010	0.0009	0.0006	0.0001
	R^2	0.982	0.981	0.983	0.981
	F_{error}	0.32	0.35	0.21	0.22
Intraparticle diffusion model	K_{id} (mg/(g-min $^{1/2}$))	0.33	0.28	0.18	0.12
	C (mg/g)	1.25	2.16	3.71	4.42
	R^2	0.911	0.952	0.941	0.893
	F_{error}	0.51	0.48	0.61	0.72

Table 5. The results show that the ΔG° values at the studied temperature are negative. The negative values of ΔG° indicate the tendency of the adsorption process to be spontaneous, and there is a high tendency of dairy wastewater

molecules for adsorption by the adsorbent. The positive value of ΔS° indicates an increase in the system randomness at the solid/liquid interface with some structural changes in the adsorbent and adsorbate. Also, the positive value of

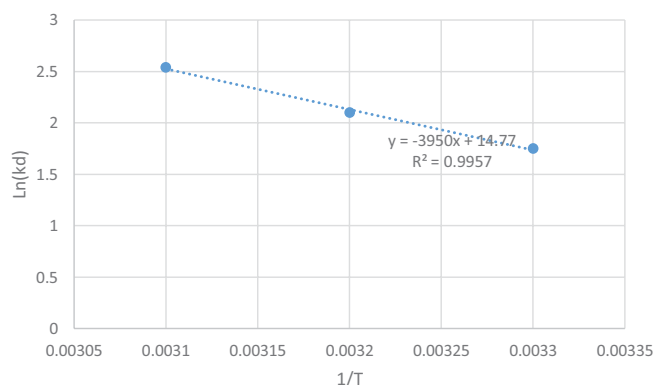


Fig. 13. Relation between thermodynamic equilibrium coefficient and temperature in dairy wastewater adsorption onto graphene/PDMS coated Fe_3O_4 MNPs.

Table 5
Thermodynamic analysis data at different temperature

	$\Delta G^\circ \left(\frac{\text{kJ}}{\text{mol}} \right)$			$\Delta H^\circ \left(\frac{\text{kJ}}{\text{mol}} \right)$	$\Delta S^\circ \left(\frac{\text{kJ}}{\text{mol}} \right)$
298	308	318		32.81	122.79
-4.33	-5.37	-6.73			

ΔH is indicative of an endothermic process. This result is entirely consistent with the previous results of increasing the adsorption with increasing temperature.

4. Conclusion

In this study, a new type of graphene/PDMS coated magnetic Fe_3O_4 nanoparticles as the adsorbent was fabricated to adsorption of organic pollutants from dairy wastewater. The resulting magnetic nanoparticles were characterized by SEM, FTIR spectroscopy, VSM, and BET. SEM micrographs revealed that the graphene containing polymeric network coated the magnetite particles. The FTIR spectra showed adsorption bands attributed to the functional groups of polymeric network, graphene, and also the Fe–O bonds of magnetite. The nitrogen adsorption/desorption (BET) analysis confirms the slit-like and non-uniform size structures of the adsorbent, which suggest the mesoporous structure. According to VSM analysis, for both prepared nanoparticles (coated and non-coated), the magnetization reduces from plateau state to zero on the removal of the magnetic field, which is evidence that the prepared nanoparticles are superparamagnetic. Also, by comparing the parameters of M_s , M_r , and C_p for coated and non-coated adsorbents, it is revealed that the magnetic properties of nanoparticles after coating were reduced by comparing the values of nude nanoparticles. Adsorption of organic pollutants from dairy wastewater was conducted in an aqueous medium at different pH values, temperatures, contact times, and initial COD concentrations. According to experimental data, the phenomenon of adsorption was favored at a higher temperature and lower pH in this case. Maximum removal as high as 98.5% could be achieved using an adsorbent dosage of 25 g/L, pH of 2,

and temperature of 45°C. Results show that the adsorption kinetic follows pseudo-second-order kinetic model, and the isothermal adsorption models fit Liu model well. The thermodynamic parameters suggested that not only was the adsorption by graphene/PDMS coated magnetic Fe_3O_4 nanoparticles spontaneous and exothermic in nature, but also the negative entropy change indicated an enthalpy driven process. Therefore, the graphene/PDMS coated magnetic Fe_3O_4 nanoparticles can be introduced as a potential adsorbent in dairy wastewater treatment.

References

- [1] N.M. Al-Anazeh, Treatment of wastewater from a dairy plant by adsorption using synthesized copper oxide nanoparticles: kinetics and isotherms modeling optimization, *Water Sci. Technol.*, 83 (2021) 1591–1604.
- [2] D. Karadag, O.E. Koroğlu, B. Ozkaya, M. Cakmakci, A review on anaerobic biofilm reactors for the treatment of dairy industry wastewater, *Process Biochem.*, 50 (2015) 262–271.
- [3] B. Mohebrad, Gh. Ghods, A. Rezaee, Dairy wastewater treatment using immobilized bacteria on calcium alginate in a microbial electrochemical system, *J. Water Process Eng.*, 46 (2022) 102609, doi: 10.1016/j.jwpe.2022.102609.
- [4] A. Kusmayadi, P.-H. Lu, C.-Y. Huang, Y.K. Leong, H.-W. Yen, J.-S. Chang, Integrating anaerobic digestion and microalgae cultivation for dairy wastewater treatment and potential biochemicals production from the harvested microalgal biomass, *Chemosphere*, 291 (2022) 133057, doi: 10.1016/j.chemosphere.2021.133057.
- [5] N. Amaly, P. Pandey, A.Y. El-Moghazy, G. Sun, P.K. Pandey, Cationic microcrystalline cellulose – montmorillonite composite aerogel for preconcentration of inorganic anions from dairy wastewater, *Talanta*, 242 (2022) 123281, doi: 10.1016/j.talanta.2022.123281.
- [6] E. O'Connor, O.N. Kavanagh, D. Chovan, D.G. Madden, P. Cronin, A.B. Albadarin, G.M. Walker, A. Ryan, Highly selective trace ammonium removal from dairy wastewater streams by aluminosilicate materials, *J. Ind. Eng. Chem.*, 86 (2020) 39–46.
- [7] S. Wang, N. Chandrasekhara Rao, R. Qiu, R. Moletta, Performance and kinetic evaluation of anaerobic moving bed biofilm reactor for treating milk permeate from dairy industry, *Bioresour. Technol.*, 100 (2009) 5641–5647.
- [8] B.S. Shete, N.P. Shinkar, Dairy industry wastewater sources, characteristics & its effects on environment, *Int. J. Curr. Eng. Technol.*, 3 (2013) 1611–1615.
- [9] Y. Shi, T. Liu, S. Chen, X. Quan, Accelerating anaerobic hydrolysis acidification of dairy wastewater in integrated floating-film and activated sludge (IFFAS) by using zero-valent iron (ZVI) composite carriers, *Biochem. Eng. J.*, 177 (2022) 108226, doi: 10.1016/j.bej.2021.108226.
- [10] P. Kumar Sharma, K. Rausa, A. Rani, S. Mukherjee, M. Kumar, Biopurification of dairy farm wastewater through hybrid constructed wetland system: groundwater quality and health implications, *Environ. Res.*, 200 (2021) 111426, doi: 10.1016/j.envres.2021.111426.
- [11] G.J. Miiito, P. Ndegwa, F.P. Alege, S.S. Coulibaly, R. Davis, J. Harrison, A vermifilter system for reducing nutrients and organic-strength of dairy wastewater, *Environ. Technol. Innovation*, 23 (2021) 101648, doi: 10.1016/j.eti.2021.101648.
- [12] W. Finnegan, J. Goggins, E. Clifford, X. Zhan, Global warming potential associated with dairy products in the Republic of Ireland, *J. Cleaner Prod.*, 163 (2017) 262–273.
- [13] A. Essecri, A. Hsini, Y. Naciri, M. Laabd, Z. Ajmal, M. El Ouardi, A.A. Addi, A. Albourine, Novel citric acid-functionalized brown algae with a high removal efficiency of crystal violet dye from colored wastewaters: insights into equilibrium, adsorption mechanism, and reusability. *Int. J. Phytorem.*, 23 (2021) 336–346.

- [14] S. Alimoradi, R. Faraj, A. Torabian, Effects of residual aluminum on hybrid membrane bioreactor (coagulation-MBR) performance, treating dairy wastewater, *Chem. Eng. Process. Process Intensif.*, 133 (2018) 320–324.
- [15] M. Jabari, Kinetic mass transfer adsorption model for treating dairy wastewater with stone cutting solid waste, *Environ. Technol. Innovation*, 7 (2017) 21–29.
- [16] M. Sharma, M. Joshi, S. Nigam, D.K. Avasthi, R. Adelung, S.K. Srivastava, Y.K. Mishra, Efficient oil removal from wastewater based on polymer coated superhydrophobic tetrapodal magnetic nanocomposite adsorbent, *Appl. Mater. Today*, 17 (2019) 130–141.
- [17] K. Wang, J. Fu, Sh. Wang, M. Gao, J. Zhu, Z. Wang, Q. Xu, Polydopamine-coated magnetic nanochains as efficient dye adsorbent with good recyclability and magnetic separability, *J. Colloid Interface Sci.*, 516 (2018) 263–273.
- [18] L. Yu, G. Hao, J. Gu, S. Zhou, N. Zhang, W. Jiang, $\text{Fe}_3\text{O}_4/\text{PS}$ magnetic nanoparticles: synthesis, characterization and their application as sorbents of oil from wastewater, *J. Magn. Mater.*, 394 (2015) 14–21.
- [19] H. Heidari, H. Razmi, A. Jouyban, Preparation and characterization of ceramic/carbon coated Fe_3O_4 magnetic nanoparticle nanocomposite as a solid-phase microextraction adsorbent, *J. Chromatogr. A*, 1245 (2012) 1–7.
- [20] B. Ekka, I. Mierina, T. Juhna, K. Kokina, M. Turks, Synergistic effect of activated charcoal and chitosan on treatment of dairy wastewaters, *Mater. Today Commun.*, 31 (2022) 103477, doi: 10.1016/j.mtcomm.2022.103477.
- [21] U. Pathak, P. Das, P. Banerjee, S. Datta, Treatment of wastewater from a dairy industry using rice husk as adsorbent: treatment efficiency, isotherm, thermodynamics, and kinetics modelling, *Int. J. Thermodyn.*, 2 (2016) 1–7.
- [22] F. Falahati, M. Baghdadi, B. Aminzadeh, Treatment of dairy wastewater by graphene oxide nano-adsorbent and sludge separation, using in situ sludge magnetic impregnation (ISSMI), *Pollution*, 4 (2018) 29–41.
- [23] N. Al-Ananzeh, Treatment of wastewater from a dairy plant by adsorption using synthesized copper oxide nanoparticles: kinetics and isotherms modeling optimization, *Water Sci. Technol.*, 83 (2021) 1591–1604.
- [24] M.D.G. de Luna, E.D. Flores, M.C.B. Cenia, M.C. Lu, Removal of copper ions from aqueous solution by adlai shell (*Coix lacryma-jobi* L.) adsorbents, *Bioresour. Technol.*, 192 (2015) 841–844.
- [25] L. Girardo, J.C. Moreno-Piraján, Study on the adsorption of heavy metal ions from aqueous solution on modified SBA-15, *Mater. Res.*, 16 (2013) 745–754.
- [26] S. Baharin, N. Muhamad Sarih, S. Mohamad, S. Shahabuddin, K. Sulaiman, A. Ma'amor, Removal of endocrine disruptor di-(2-ethylhexyl) phthalate by modified polythiophene-coated magnetic nanoparticles: characterization, adsorption isotherm, kinetic study, thermodynamics, *RSC Adv.*, 6 (2016) 44655–44667.
- [27] Y. Yao, S. Miao, S. Liu, L.P. Ma, H. Sun, S. Wang, Synthesis, characterization, and adsorption properties of magnetic $\text{Fe}_3\text{O}_4/\text{graphene}$ nanocomposite, *Chem. Eng. J.*, 184 (2012) 326–332.
- [28] C.H. Weng, Y.T. Lin, T.W. Tzeng, Removal of methylene blue from aqueous solution by adsorption onto pineapple leaf powder, *J. Hazard. Mater.*, 170 (2009) 417–424.
- [29] H. Qiu, L. Lv, B. Pan, Q.J. Zhang, W. Zhang, Q.X. Zhang, Critical review in adsorption kinetic models, *J. Zhejiang Univ. A*, 10 (2009) 716–724.
- [30] V.V.C. Lima, F.B.D. Nora, E.C. Peres, G.S. Reis, É.C. Lima, M.L.S. Oliveira, G.L. Dotto, Synthesis and characterization of biopolymers functionalized with APTES (3-aminopropyltriethoxysilane) for the adsorption of sunset yellow dye, *J. Environ. Chem. Eng.*, 7 (2019) 103410, doi: 10.1016/j.jece.2019.103410.
- [31] G.S. dos Reis, B.G. Cazacliu, C.R. Correa, E. Ovsyannikova, A. Kruse, C.H. Sampaio, E.C. Lima, G.L. Dotto, Adsorption and recovery of phosphate from aqueous solution by the construction and demolition wastes sludge and its potential use as phosphate-based fertiliser, *J. Environ. Chem. Eng.*, 8 (2020) 103605, doi: 10.1016/j.jece.2019.103605.
- [32] I.H. Khalaf, F.T. Al-Sudani, A.A. Abdul Razak, T. Aldahri, S. Rohani, Optimization of Congo red dye adsorption from wastewater by a modified commercial zeolite catalyst using response surface modeling approach, *Water Sci. Technol.*, 83 (2021) 1369–1383.
- [33] Saruchi, V. Kumar, Adsorption kinetics and isotherms for the removal of Rhodamine B dye and Pb^{2+} ions from aqueous solutions by a hybrid ion-exchanger, *Arabian J. Chem.*, 12 (2019) 316–329.
- [34] H.A. Alalwan, M.M. Mohammed, A.J. Sultan, M.N. Abbas, T.A. Ibrahim, H.A.S. Aljaafari, A.A. Alminshid, Adsorption of methyl green stain from aqueous solutions using non-conventional adsorbent media: isothermal kinetic and thermodynamic studies, *Bioresour. Technol.*, Rep., 14 (2021) 100680, doi: 10.1016/j.biteb.2021.100680.
- [35] M. Ponnuchamy, A. Kapoor, B. Pakkirisamy, P. Sivaraman, K. Ramasamy, Optimization, equilibrium, kinetic and thermodynamic studies on adsorptive remediation of phenol onto natural guava leaf powder, *Environ. Sci. Pollut. Res.*, 27 (2020) 20576–20597.
- [36] H.L. Chieng, L.B.L. Lim, N. Priyantha, Sorption characteristics of peat from Brunei Darussalam for the removal of Rhodamine B dye from aqueous solution: adsorption isotherms, thermodynamics, kinetics and regeneration studies, *Desal. Water Treat.*, 55 (2015) 664–677.